Available online at www.sciencedirect.com
SCIENCE DIRECT®
International Journal of Heat and Mass Transfer 48 (2005) 4797–4810
International Journal of HEAT and MASS TRANSFER
www.elsevier.com/locate/ijhmt

Boiling nucleation and two-phase flow patterns in forced liquid flow in microchannels

J. Li, G.P. Peterson *

Department of Mechanical, Aerospace and Nuclear Engineering, Rensselaer Polytechnic Institute, 110 8th Street, Troy, NY 12180, USA

Received 10 March 2005; received in revised form 12 May 2005
Available online 10 August 2005

Abstract

Using microfabrication techniques, a microscale platinum heater was fabricated on a Pyrex glass wafer and located in a shallow, but nearly trapezoidal microchannel with a hydraulic diameter of $D_h = 56$ microns fabricated on another glass wafer. Using a high-speed digital CCD video camera and microscope, the boiling nucleation temperature and two-phase flow patterns were observed and examined at different mass flow rates. The nucleation temperature was found to be reasonably close to the theoretical values as predicted by a 3D numerical heat transfer simulation with the measured bulk temperature of the microheater. The stability of the developed flow indicated three clearly distinguishable two-phase flow regimes: bubbly, wavy and annular. To avoid problems observed in the past, care was taken to ensure that the results were not influenced by the entrance and/or exit regions of the test section. The observed variations in the two-phase flow patterns were compared with the results of a model developed using a stability analysis of the liquid film.

Keywords: Nucleation; Two-phase flow; Flow pattern; Stability; Microchannel

1. Introduction

Phase change heat transfer presents an optimal mechanism for the removal of excess heat from electronic devices and microelectronic systems. The high latent heat occurring in this phase change phenomenon results in a small increase in temperature and presents a number of other independent advantages. Most important among these is that the flow boiling produces only a modest increase in the device temperature, even at extremely high heat fluxes, which directly corresponds to a large increase in the amount of heat removed from the system. While determination of the two-phase liquid/vapor flow pattern is critical for the design of microchannel two-phase flow heat sinks, there exists significant differences in the observations and results as measured by various investigators.

Peng and Wang [1] suggested that it was extremely difficult to generate bubbles, even at a very high heat flux in a microchannel. They hypothesized that in a microchannel, small bubble embryos could form, but since they cannot grow to the critical bubble radius, r_c, formulated by conventional nucleation theory, the nucleated bubbles will eventually collapse [2]. In Wu and Cheng's

* Corresponding author. Tel.: +1 518 276 6487; fax: +1 518 276 4061.
E-mail address: peterson@rpi.edu (G.P. Peterson).

0017-9310/$ - see front matter © 2005 Elsevier Ltd. All rights reserved.
doi:10.1016/j.ijheatmasstransfer.2005.05.029

experimental studies [3], bubbly flow, slug flow, churn flow and annular flow were all observed in trapezoidal microchannels with hydraulic diameters of 186, 158.8 and 82.8 μm. These studies, also found that once boiling heat transfer in the microchannel was established, two-phase flow and single-phase liquid flow appeared alternatively within the channel, with large-scale variations in the temperature of the substrate and fluid, and differences in the pressure and mass flow rate of the fluid [4]. Lee et al. [5], fabricated an integrated rectangular microchannel heat sink, and observed that annular flow in rectangular microchannels is unstable and the dominant flow pattern in an unsteady transition region connecting the upstream vapor zone to the downstream liquid zone varies with the average location and the input power. They also hypothesized that based upon previous studies, annular flow was established at a relatively low power input and suppressed the development of bubbly flow [6]. Hetsroni et al. [7] performed air–water and steam–water flow in parallel triangular microchannels. In the resulting steam–water flow, instability in uniformly heated microchannels was observed.

Only two studies have been found in which systematic investigations of the two-phase flow patterns in microchannel flow have been investigated. Chung et al. [8] conducted an adiabatic experiment to investigate the effect of channel geometry on gas–liquid two-phase flow characteristics in horizontal 96 μm square microchannels and 100 μm circular channels. However, in these gas–liquid two-phase flow experiments, only slug flow was observed. Bubbly and annular flow along with other possible flow regimes were not observed for the flow conditions tested. Qu et al. [9] also conducted tests using gas/liquid two-phase flow in microchannels. In this investigation, the dominant flow patterns observed were slug and annular, with bubbly flow occurring only occasionally; stratified and wavy flows were never observed.

To summarize the above literature, to date, no systematic investigations of the various vapor–liquid two-phase flow regimes have been found in the literature. Because the shape and size of the inlet and outlet plenums of the microchannels have been shown to influence the stability of the two-phase flow [3–7,10–12], it is entirely plausible that the observed flow patterns in the previously discussed investigations are the result of the design of the test facility, in which the vapor phase or the vapor/liquid two-phase is significantly influenced by the entrance or exit region, rather than the inherent nature of the microchannel two-phase flow. In an effort to resolve some of the questions surrounding the two-phase flow regimes in microchannels and the influence of the various parameters on these flow regimes, a unique experimental approach was designed to explore the phase change mechanisms and how they affect the flow regimes in microchannels. Using MEMS based technology, a microscale platinum heater was fabricated on a Pyrex glass wafer and a shallow but nearly trapezoidal microchannel fabricated on another wafer with hydraulic diameter of 56 μm were bonded together. Then, using

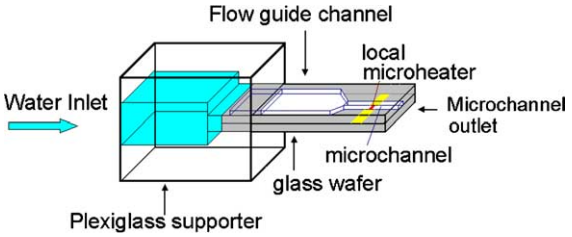

Fig. 1. The test section.

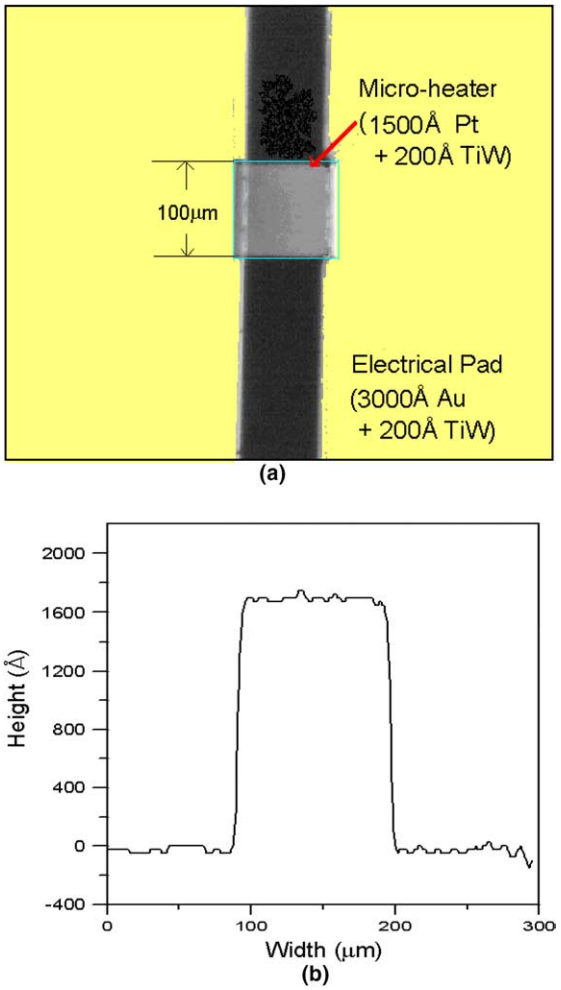

Fig. 2. The fabricated microheater test article. (a) Photomicrograph of the microheater and the electrical pad, (b) surface roughness of the microheater.

a high-speed digital video camera, the two-phase flow patterns as a function of the local vapor generation could be explored and recorded with a microscope and a high-speed CCD digital camera. The impact of the *size of the microchannel* and the *flow rate* on the incipience of the vapor generation and the two-phase flow patterns were then analyzed. Through a series of experiments, it was found that the instability associated with the phase change is not obvious and the different two-phase flow patterns are distinguished from each other and stable under certain power input and mass flow rates. By comparing the experimental observations with the results of a 3D numerical heat transfer simulation, the boiling incipience temperature was found to be quite close to the theoretically predicted value obtained from the classical kinetics of boiling. In the following, a mechanism based on the stability analysis of liquid film is proposed, and used to reveal the shape and resulting flow regimes of the vapor column under different flow conditions.

2. Device design and microfabrication

The test section is illustrated in Fig. 1. The test section includes a plexiglass support, into which a pressure transmitter and thermocouple are attached, along with the experimental test article, constructed from two Pyrex wafers onto which a microchannel and a small micro heater have been fabricated separately and bonded together by epoxy glue after alignment and fixing. In this design of the test section, a very long single microchannel with a well designed, smooth entrance region and an outlet that is open to the environment in order to avoid any influence from the plenum or chamber connected to the outlet of the microchannel as used previously are adapted.

The microheater used in the current investigations is illustrated in Fig. 2(a) and was fabricated using MEMS based technology and a typical lift-off metallization application. A 200 Å TiW film (for adhesion) and 1500 Å platinum film are sputtered onto a Pyrex glass wafer coated with photoresist after the photolithography process. After lift-off in acetone, a similar process is repeated for a gold pad with a thickness of 3000 Å and 200 Å for TiW. The width and length of the platinum microheater are both 100 μm. The length and width of the gold pad are 10 and 2 mm, respectively, on each side.

The surface roughness of the microheater was measured using a scanning profilometer and is described in

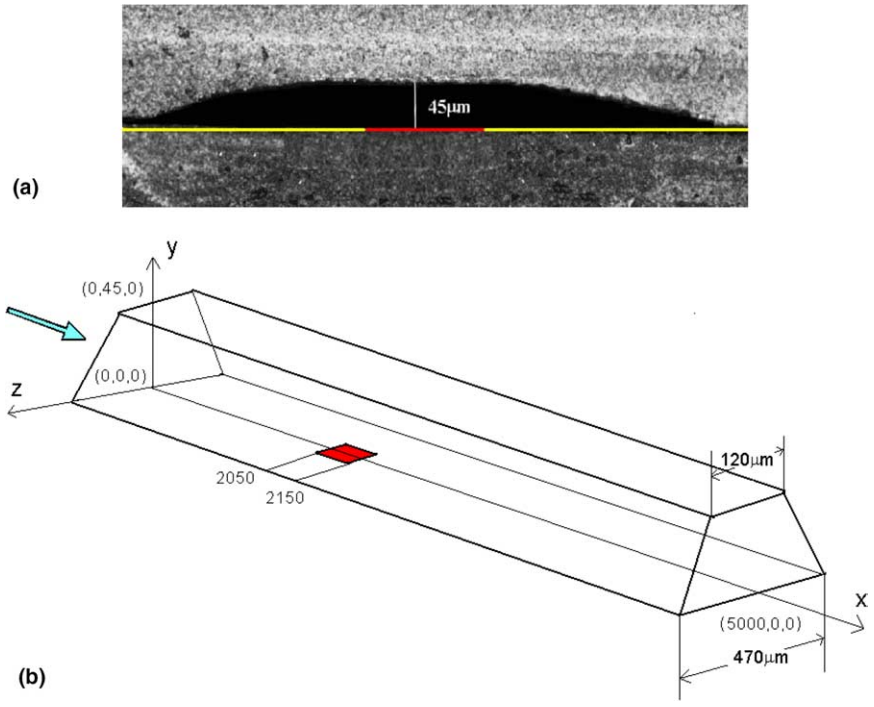

Fig. 3. The fabricated microchannel and the test article configuration. (a) Cross-section of the microchannel (the dark line at the bottom of the channel is the platinum microheater and the white line is the gold electrical pad) and (b) geometry of the channel and position of the microheater (the arrow indicates the flow direction).

Fig. 2(b). The average roughness of the microheater was approximately 50 Å (5 nm). This roughness is in the range of the critical bubble size for homogeneous bubble nucleation and thus can help to avoid the influence of cavity size on bubble nucleation.

The microchannel and flow guide channels were fabricated using a wet etching technique. The fabricated microchannel is illustrated in Fig. 3(a). To accomplish this, the sides of the glass wafer were covered with a 200 Å thick layer of TiW and a 2000 Å thick layer of Au using a metal sputtering technique. After applying the pattern with a photoresist coating and the photolithography process, the wafer was immersed into a $KI:I_2:H_2O$ solution for gold etching and a hydrogen peroxide solution for TiW etching. Then using the metal pattern as the mask, the channels were fabricated by dipping the wafer into a diluted HF solution (Concentrated HF(49%):Water = 1:1). Finally, the metal coating was removed to expose the glass wafer.

As shown in Fig. 3, the width of the fabricated microchannel is approximately 120 μm (top) and 470 (bottom), and the microchannel height is 45 μm. The configuration of the test specimen is shown in Fig. 3(b).

3. Experimental test facility and procedures

The experimental test facility is illustrated in Fig. 4, and includes a water circulating unit, a heating unit, a data acquisition unit, and the test section. Deionized, distilled water is pumped from a tank by a micropump and flows successively through a valve, a 2 μm filter, a flow rate sensor, a Plexiglas support in which a pressure transducer and a thermocouple have been inserted and finally to the test specimen. The heating unit utilizes a DC power supply and an electronic control circuit, with which the total voltage input supplied to the microheater can be adjusted and controlled, and through which the trigger signal can be produced. This trigger signal activates the data acquisition unit, which is comprised of a digital oscilloscope to monitor and record the inlet pressure from the pressure transmitter, a flow sensor to determine the flow rate, and a voltage input transducer to control the microheater. A microscope with the maximum magnification of 500× and a high-speed digital CCD camera with a maximum recording rate of 2000 fps were used to observe and record the flow patterns occurring in the microchannels. The test section

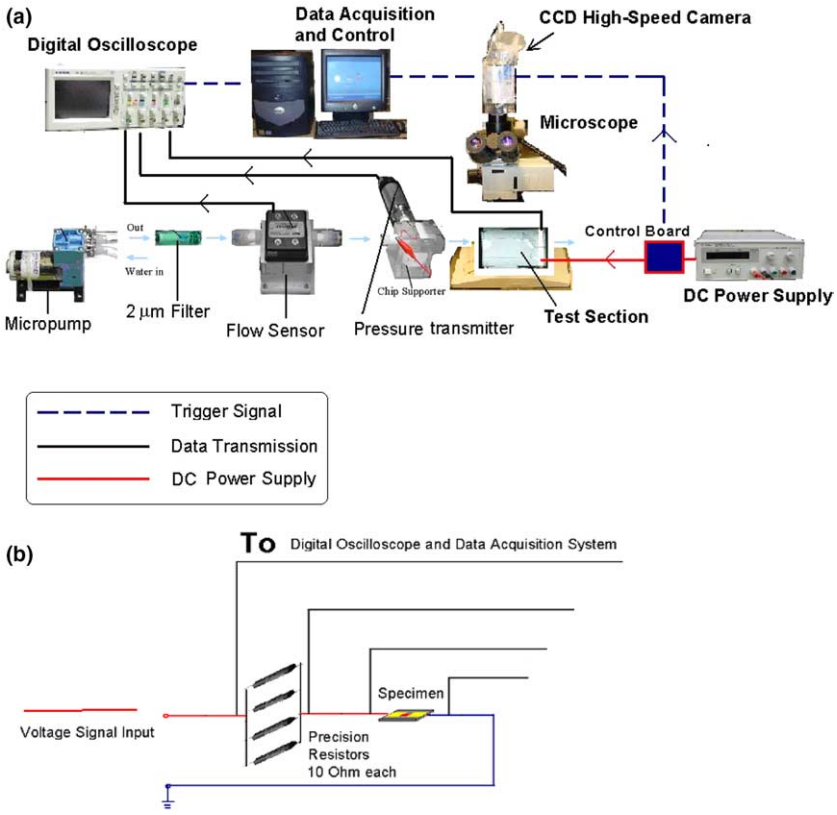

Fig. 4. The experimental system. (a) Experimental test facility and (b) resistance measurement circuit.

included a Plexiglas support, to hold the chip and to monitor the pressure and temperature; a Petri-dish catch vessel, to measure the mass flow rate; and the fabricated test specimen. The uncertainties of the flow sensor, the pressure transmitter, and the balance used to determine the flow rate, have been determined to be ± 1%, ± 0.2% and ± 0.01%, respectively.

The temperature of the microheater was obtained from the relationship between the temperature and the resistance. The resistance measurement of the microheater during the experimental tests are shown in Fig. 4(b). By placing the microheater in the thermal bath and/or on a hot plate, and isolating it with a cover to reduce the oscillation of the temperature, the relationship between the resistance and the temperature of the microheater can be determined and calibrated. The result of this calibration procedure is shown in Fig. 5. A linear fit was applied to the calibration data and the gradient of the curve fit was 0.00379 Ω/°C, as shown in Fig. 5. The temperature difference between the two thermocouples attached to the microheater specimen used for calibration was limited to less than 0.1 °C difference and the accuracy of the digital multimeters was maintained at four significant digits during the microheater sensor calibration. The calibration results indicated a relationship between the bulk temperature and the resistance of the microheater given as

$$R_{pt}(T_{bulk}) = R_0 \cdot f[R_{pt}(T_{bulk})] = 1.6361 \times [1 + 0.002316 \cdot (T_{bulk} - 273.15)] \quad (1)$$

As discussed in the introduction, the vapor nucleation temperature and the two-phase flow patterns under different liquid flow rates are the principal topic of interest in this investigation. An approximate temperature rise rate of 10 K/s in the microheater was established to heat the liquid with a prefixed constant flow rate. Once the boiling had been initiated, the total voltage input was kept constant in order to explore the vapor stem behavior and two-phase flow pattern.

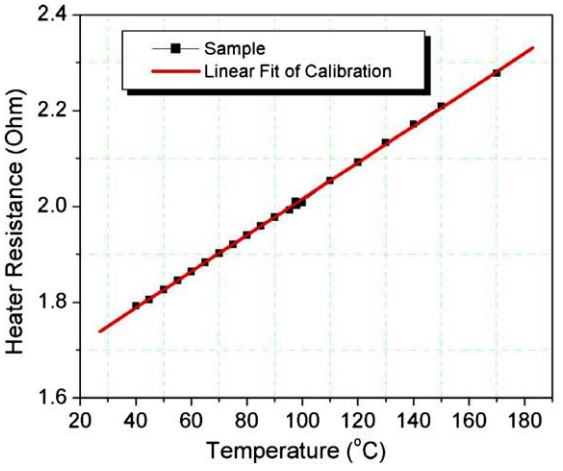

Fig. 5. Calibration of the microheater test article.

4. Experimental results

4.1. Low mass flow rate and bubbly flow

Fig. 6 illustrates the variation of the power consumed and the bulk temperature of the microheater as a function of time for a flow rate of 35 g/mm^2 min ($Re_D = 37.1$), and a power input of approximately 0.43 W. At these conditions, a stable bubbly flow was observed in the microchannel and the boiling incipience temperature was found to be 210 °C for this relatively low mass flow rate. As shown, once the boiling incipience temperature had been reached, the temperature of the microheater decreased slightly due to the enhanced heat transfer resulting form the phase change. As the size of the vapor bubble increased, the temperature of the microheater increased, until the heat power input and vapor generation rate had reached equilibrium. As the temperature of the microheater increased, the resistance also increased, and thus the voltage drop across the microheater increased (refer to Fig. 4(b)). This

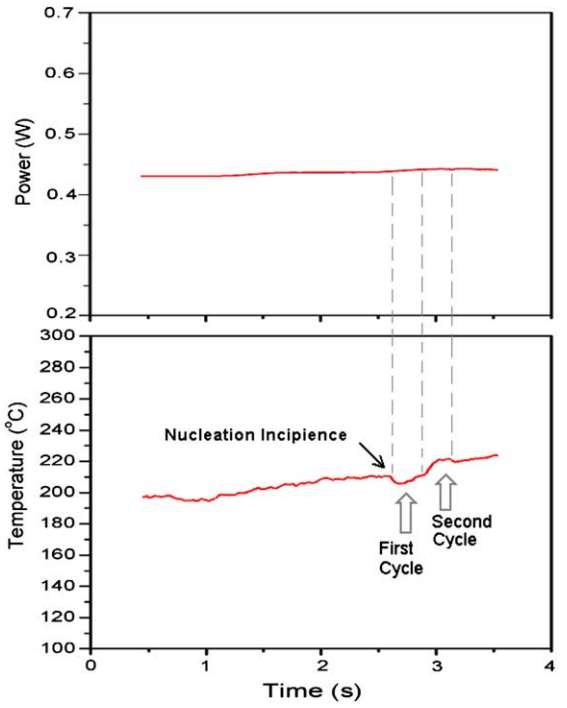

Fig. 6. Variation of the power consumed and the bulk temperature of the microheater as a function of time for a flow rate of 35 g/mm^2 min.

resulted in a concomitant increase in the power consumed by the microheater.

Fig. 7 presents photomicrographs of the vapor generation and bubble dynamics recorded using the high-speed digital imaging system. As illustrated in Fig. 7(a), immediately following the onset of boiling, i.e., at a time of 0.004 s the rate of bubble growth accelerated rapidly. This can be attributed to the vapor explosion occurring on the smooth surface of the heater. As a result of the non-equilibrium that exists between the internal vapor pressure and the surrounding liquid, the vapor bubble (or vapor column) grows steadily from a dynamics governing stage ($\leqslant 0.048$ s) to a heat transfer governing stage (>0.048 s). When the surface tension is no longer sufficient to withstand the stresses exerted by the flowing liquid on the bubble interface, the main vapor column detaches from the microheater and is swept away by the liquid flow. The remaining vapor on the microheater then serves as the origin for the next bubble, as shown in Fig. 7(b). Prior to detachment, the bubble is stretched into a long tear-like shape and then ultimately progresses to a gourd shape due to the surface tension. This cycle of bubble growth and detachment continues at regular intervals and appears to be quite stable.

4.2. Moderate mass flow rate and wavy flow

If the mass flow rate of the liquid is increased to a moderate flow rate or approximately 112 g/mm^2 min ($Re_D = 117.6$) and the input power is incremented to a value of 0.6 W, a stable wavy vapor column is formed in the microchannel. Fig. 8 illustrates the variation of the power consumed in the microheater and the bulk temperature of the microheater as a function of time. For these conditions, the boiling incipience temperature was 190 °C. Following boiling incipience, the temperature of the microheater again decreased slightly, due to the enhanced heat transfer resulting from the phase change. As discussed previously, as the size of the vapor bubble increased, the temperature of the microheater

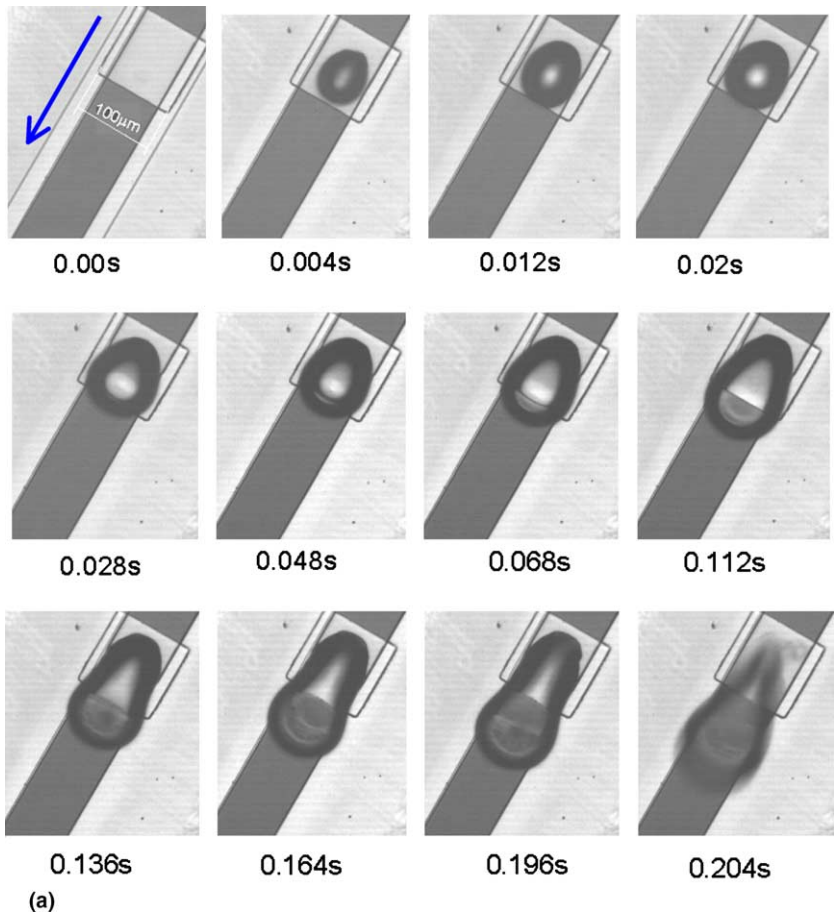

Fig. 7. High speed observation of the transient nucleation phenomena on the microheater and developing bubbly flow in the microchannel for a mass flow rate of 35 g/mm^2 min. (a) Cycle I—bubble nucleation, growth and detachment from the microheater and (b) cycle II—developing bubbly flow.

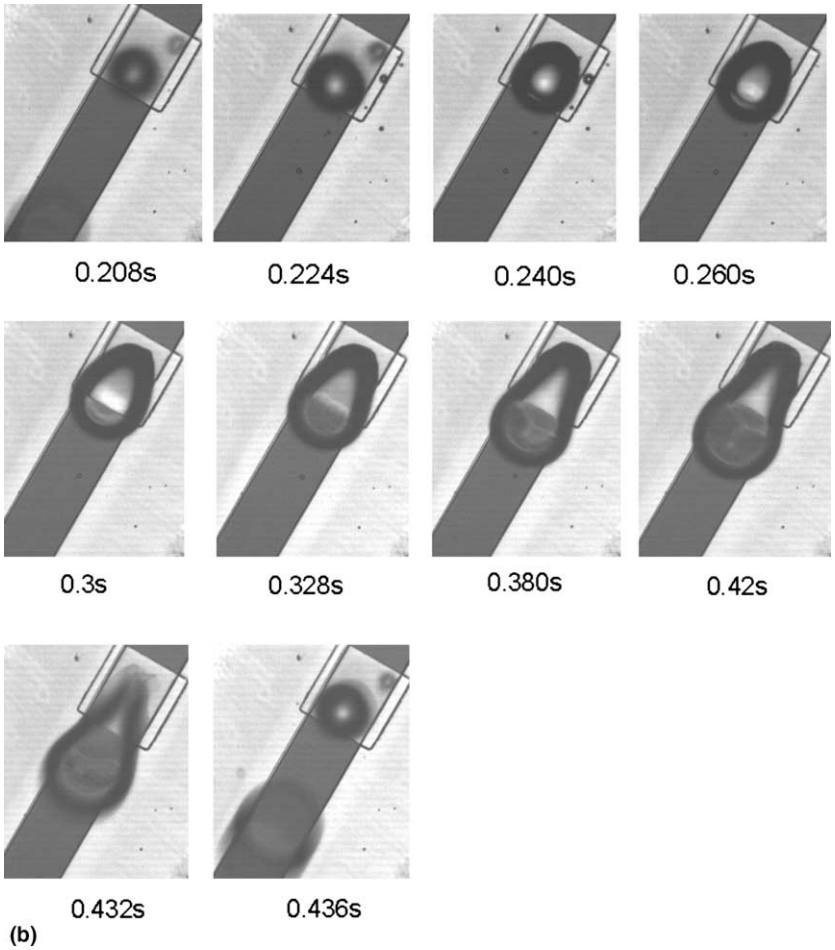

Fig. 7 (*continued*)

increased, until the heat power input and vapor generation rate had reached equilibrium resulting in an increase in the temperature of the microheater, which resulted in an increase in the resistance of the microheater and the concomitant increase in the power consumed by the microheater. Fig. 9 presents a series of photo micrographs of the transient vapor nucleation phenomena occurring on the microheater at this moderate flow rate and the resulting developing wavy flow in the microchannel. The deformation of vapor column resulting from the stresses induced by the forced liquid flow is apparent, particularly when compared with Fig. 7 for the low liquid flow rate. The wavy vapor column observed in Fig. 9 is formed and shaped by a combination of the surface tension and the stresses exerted by liquid flow surrounding the vapor column. The resulting shape, which appears to be similar to a pearl necklace with intermittent bulges and narrow regions, is apparent in Fig. 9(a). As shown in Fig. 9(b), when the drag on the wavy vapor column exceeds the surface tension forces, the bulge farthest from the heater breaks away from the main column and is carried downstream by the surrounding liquid and another similar cycle starts over again. Again, the fully developed wavy flow in the microchannel is very stable and is dominated by the surface tension. This is believed to be the first time that this type of flow pattern in microchannel two-phase flow has been reported in the literature.

4.3. High mass flow rate and annular flow

Continued increases in the mass flow rate up to 584 g/mm^2 min ($Re_D = 610.6$) with a power input of 0.7 W to the microheater, results in a stable annular flow pattern in the microchannel. Fig. 10 illustrates the variation of the power consumed in the microheater and the bulk temperature as a function of time. The measured boiling incipience temperature was 145 °C for this high mass flow rate. It should be noted that because the upstream liquid is subcooled and the measured temperature

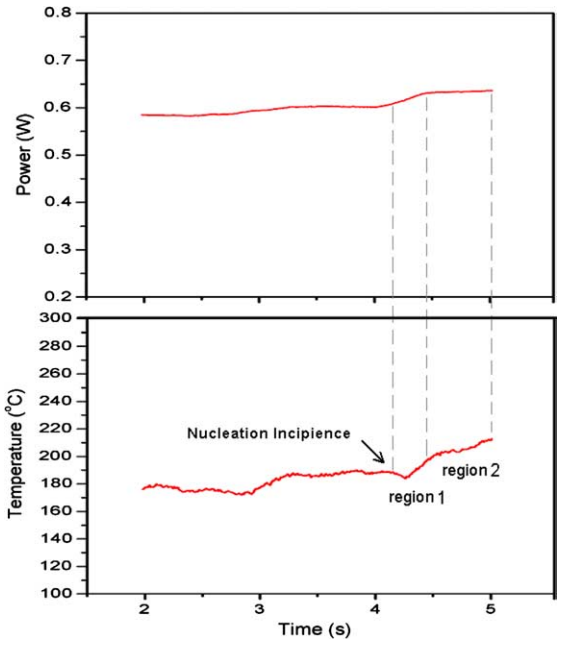

Fig. 8. Variation of the power consumed and the bulk temperature of microheater as a function of time for a flow rate of 112 g/mm^{2}min.

is the bulk temperature of the microheater, the measured value does not represent the true boiling incipience temperature. The true incipience temperature is the temperature that occurs within the hottest region of the microheater surface. This value can best be determined by a verified 3D heat transfer numerical simulation under the same mass flow rate and the input power conditions.

As was discussed in the previous cases, the temperature of the microheater decreased slightly following the onset of boiling and then increased until steady state was reached. The flow pattern or regime is illustrated in Fig. 11, which illustrates the transient vapor nucleation phenomena on the microheater and the developing annular flow in the microchannel. This annular vapor column is initiated by a bubble-shaped vapor column and grows quickly to form a stable annular vapor column, stretched to an elongated shape by the liquid flowing around the column. When the annular vapor column becomes sufficiently long, the drag force of the surrounding liquid exceeds the surface tension and a vapor bubble detaches from the main vapor column and flows downstream. An interesting phenomenon was observed when this annular flow occurred: although the downstream surface or interface of the vapor column was somewhat obscure, it appears to remain open, due to the rapidity with which the detaching vapor bubbles are being swept away.

Additional visual observation indicated that some of the vapor might be condensing at the downstream end of the annular vapor column, allowing vapor and condensate to flow downstream from the main vapor column together. This is even more apparent under higher mass flow rates. Again, however, the flow pattern was very stable.

5. Analysis and discussion

5.1. Vapor nucleation temperature

The incipience temperature for water can be computed from the classical kinetics of nucleation for different cases [13,14]:

Homogeneous

$$J_{\text{hom}} = N_0 \left(\frac{kT_{\text{nl}}}{h}\right) \exp\left[-\frac{16\pi\sigma^3}{3kT_{\text{nl}}(P_{\text{b}} - P_{\text{l}})^2}\right] \tag{2}$$

Heterogeneous

$$J_{\text{het}} = N_0^{2/3} \psi \left(\frac{kT_{\text{nl}}}{h}\right) \exp\left\{-\frac{16\pi\sigma^3\omega}{3kT_{\text{nl}}(P_{\text{b}} - P_{\text{l}})^2}\right\} \tag{3}$$

Using Eq. (2), the superheat limit for pure water was determined to be 265.8 °C (539 K for $J = 1$) [13]. The heterogeneous nucleation temperature with dissolved gases can be obtained as described by Li and Cheng [14], and the heterogeneous nucleation temperature on a smooth surface with saturated, dissolved air is approximately 231 °C with a contact angle of 20° for water on a platinum surface [15].

The vapor nucleation in this study should be attributed to the vapor explosion mechanism on a smooth surface and the boiling incipience temperature can be determined from the kinetics of nucleation. However, with the exception of the low mass flow rate case, where the measured temperature was 210 °C, the other investigated were well below the heterogeneous nucleation temperature for a smooth surface with saturated dissolved air of 231 °C.

One explanation for the difference between the theoretical value and the experimental results, especially for high flow rates, is the non-uniformity of the temperature distribution of the microheater under subcooled liquid forced flow convection. Using a 3D heat transfer numerical simulation, the temperature distribution on the microheater surface can be explored and compared to the theoretical value.

Previous investigations have demonstrated that the length required for the formation of fully developed laminar flow in channels, L_e can be estimated as $\frac{L_e}{D_h} = 0.057 Re_D$ [16]. In the current experimental investigation,

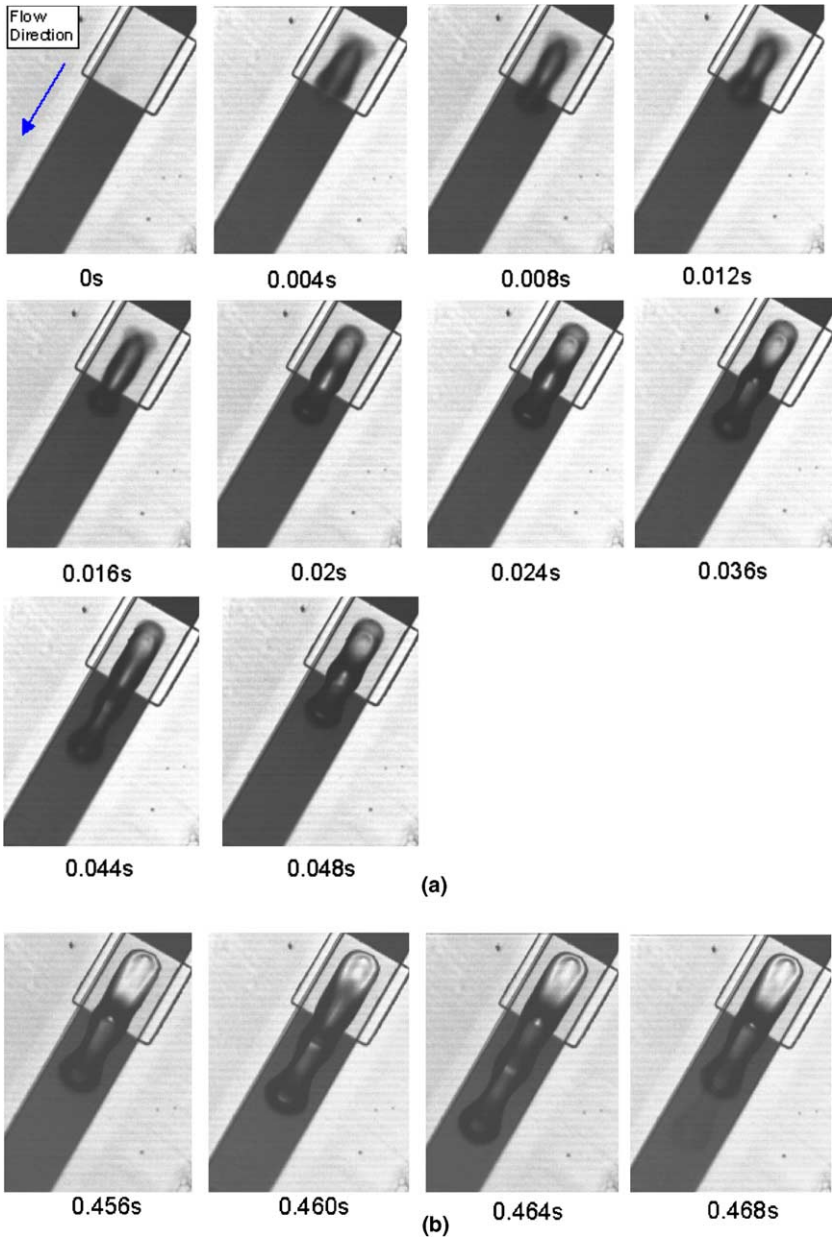

Fig. 9. High speed observation of the transient nucleation phenomena on the microheater and wavy flow developing in the microchannel for a mass flow rate of 112 g/mm^{2}min. (a) Phase I—vapor nucleation and developing wavy flow. (b) Phase II—developed wavy flow.

the upstream length was more than sufficient to ensure that the flow was fully developed, well before it reached the microheater. Fig. 12 illustrates the cross-sectional temperature distribution at $z = 0$ for three different flow rates and power inputs (note, the heater is located between 2.05 and 2.15 mm at the bottom of the channel as shown in Fig. 3(b)). Fig. 13 shows the local temperature distribution on the bottom surface of the channel and the microheater when the bulk temperature of the microheater agreed with the measured result. It is apparent here that the highest temperature on the microheater surface for different mass flow rates and input powers is somewhat higher than the average bulk temperature with the level of temperature nonuniformity dependent upon the mass flow rate of the liquid and the highest temperature is approximately 240 °C for

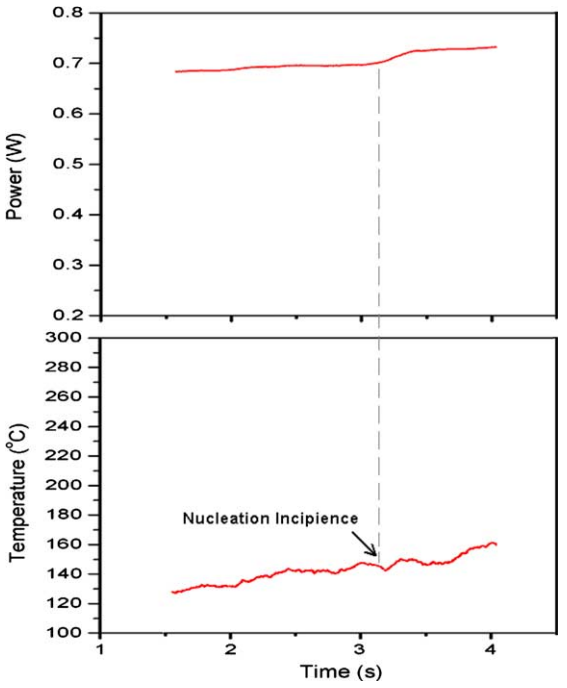

Fig. 10. Variation of the power consumed and the bulk temperature of microheater as a function of time for a flow rate of 584 g/mm^{2}min.

the low mass flow case and 250 °C for the high mass flow case, which is very close to the theoretical value of 231 °C. From this comparison, it is apparent that for a transient heating process, the vapor nucleation temperature will be close to or perhaps higher than the theoretically predicted value based upon the kinetics of nucleation.

5.2. Mechanism of two-phase flow patterns in microchannels

As previously discussed, the liquid–vapor two-phase flow patterns existing in small tubes and microchannels is an area of considerable controversy. Several different two-phase flow pattern maps in tubes have been proposed or developed by different investigators [17–21]. The underlying mechanism that governs this behavior, however, is still not well understood even in conventional tubes. As depicted in the previous sections, most of the currently available literature indicates that the flow boiling or flow condensation in microchannels is a highly unstable phenomenon that fluctuates significantly under initial constant conditions. The current investigation however indicates that the flow patterns, while significantly different are each individually stable.

After carefully examining the high-speed images and the time related temperature data a 3D vapor column shape analysis was developed as depicted in Fig. 14. It is well understood that the shape of a liquid–vapor interface is determined by the associated forces acting upon it. Principal among these is the surface Young–Laplace equation,

$$P_v - P_l = \sigma\left(\frac{1}{R_0} + \frac{1}{R_i}\right)_{i=1,2} \tag{4}$$

where P_v and P_l are the local vapor pressure and liquid pressure, respectively; and R_0 is the principal curvature of the vapor column, which depends on P_v and P_l. The secondary radii of curvature, R_1 and R_2, represent the curvature of the interface at different locations and is less sensitive to the pressure than R_0 by comparison. These values, R_1 and R_2, however, are closely related to the velocity of liquid and the rate of vapor generation. Conditions must also be such that R_1 and R_2 satisfy the stability of the thin evaporating liquid film, assuming that the surrounding liquid is a moving liquid film on the order of tens to hundreds of microns thick. If the fluid is a charge-neutral dielectric liquid [22], the governing equation for the liquid film is,

$$\rho(\mathbf{v}_t + \mathbf{v}\cdot\nabla\mathbf{v}) = -\nabla P - \nabla\phi + \mu\nabla^2\mathbf{v} \tag{5}$$

where $\mathbf{v}$ is the liquid velocity vector; P denotes the pressure in the liquid; $\Delta\phi$ is an extra body force that models the van der Waals attractions; and ϕ is the potential function, which represents the van der Waals forces and depends on the shape of the film layer,

$$\phi = \phi(h) = \phi[h(R_i)_{i=1,2}] \tag{6}$$

The shape of the film can be expressed as a function of the second curvature of the interface R_i. Combining Eq. (5) and the continuity and energy equations will result in the long-wave theory, which can be used to derive the profile of the liquid film under different situations (heating or cooling) [23]. A more detailed analysis is beyond the scope of this work. Summarizing and referring to Figs. 7, 9 and 11, respectively,

- if $R_1 = R_2 = \infty$ and $R_0 \neq 0$, and P_v is large (R_0 is small), the flow is annular flow,
- if $R_1 \approx R_2 \neq 0$ and $R_0 \neq 0$, and P_v is moderate (R_0 is moderate) the flow is wavy flow,
- if $R_1 \neq R_2$ ($R_2 > R_1$) and $R_0 \neq 0$, and P_v is small (R_0 is large), the flow is bubbly flow.

Furthermore, for bubbly flow, the detachment diameter of the bubble and the detachment frequency are connected to the bubble dynamics and the bubble shape evolution in a flow [24]. In addition, P_v is the vapor pressure and is connected to the speed of vapor generation and the speed of vapor detachment from the main vapor column: the higher the vapor pressure P_v, the

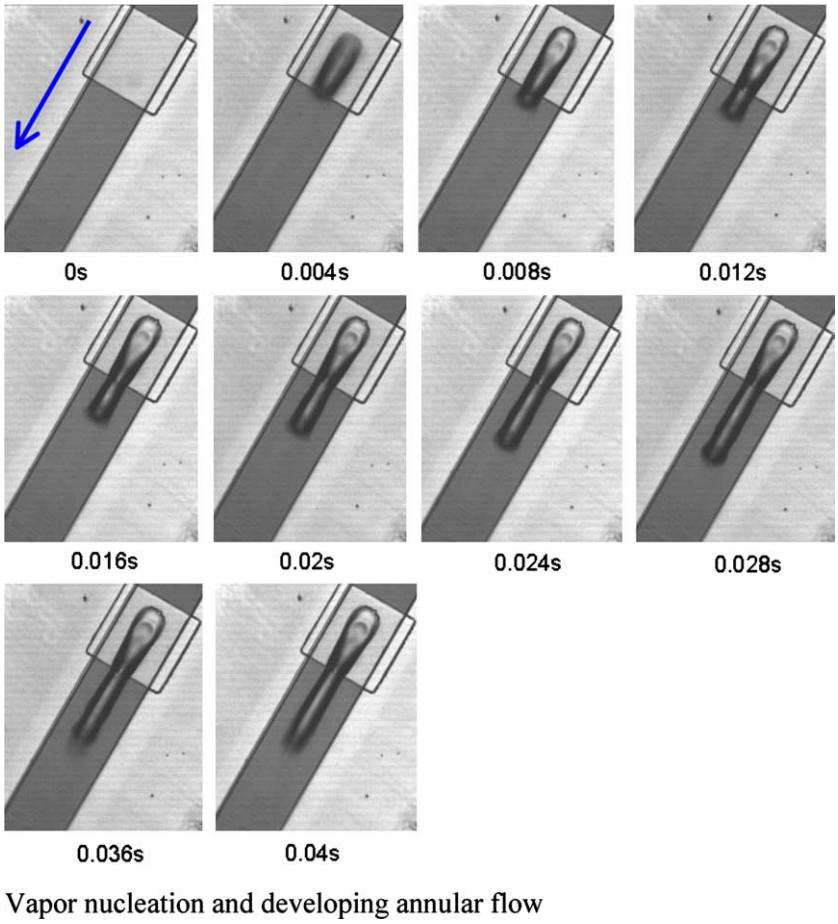

Fig. 11. High speed observation of the transient nucleation phenomena on the microheater and annular flow developing in the microchannel for a mass flow rate of 584 g/mm^2 min.

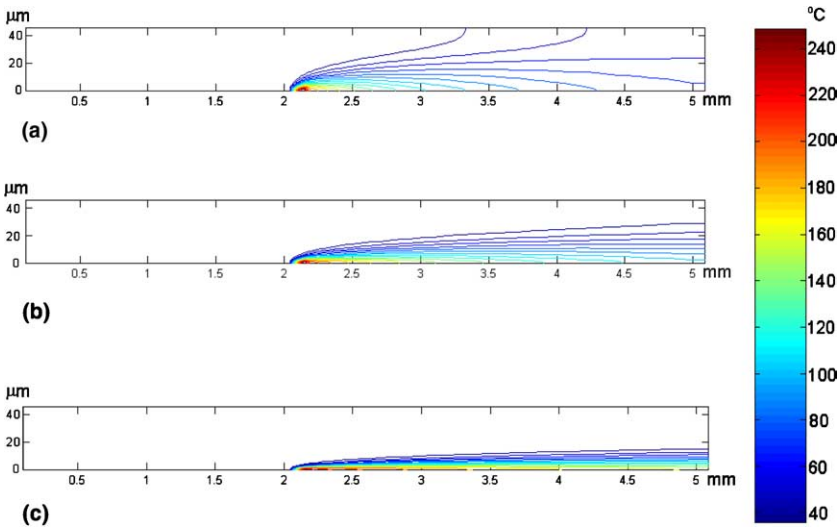

Fig. 12. 3D numerical results of the cross-sectional temperature distribution at $z = 0$ for different flow mass rates and input powers. (a) Low mass flow rate: 35 g/mm^2 min, (b) moderate mass flow rate: 112 g/mm^2 min, (c) high mass flow rate: 584 g/mm^2 min.

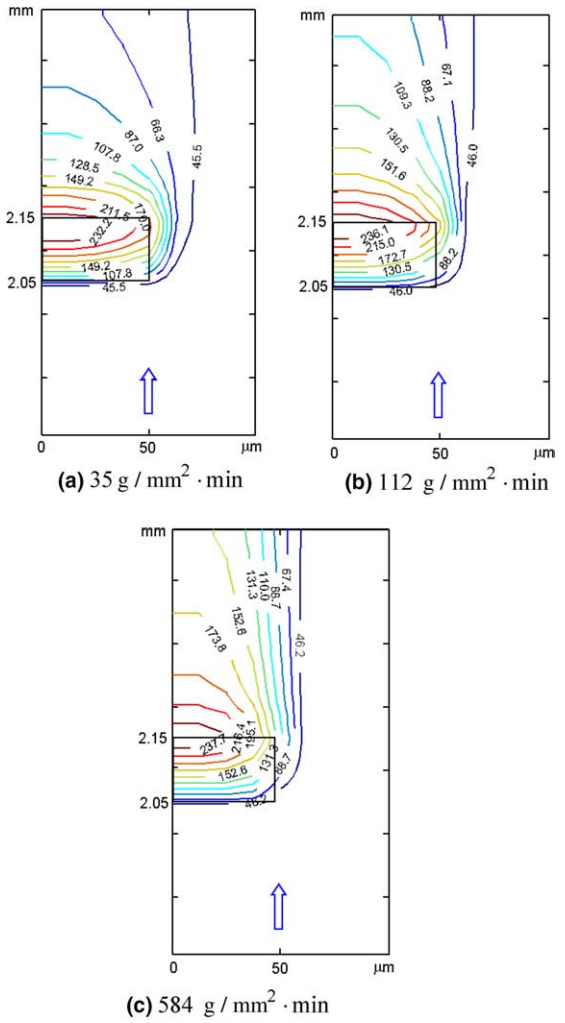

Fig. 13. 3D numerical results indicating the local temperature distribution on the top surface of the microheater for different mass flow rates with an averaged bulk temperature of (a) 210 °C for 35 g/mm^2 min, (b) 190 °C for 112 g/mm^2 min, (c) 145 °C for 584 g/mm^2 min, respectively.

faster the movement of the vapor. The vapor pressure, P_v, is also connected to the temperature of the microheater, where the higher the temperature of the microheater, the higher the vapor pressure. From the different principal curvatures, R_0, of the vapor column as shown in Figs. 7, 9 and 11 and Eq. (4), it can be deduced that the highest temperature of the microheater for case 3 is slightly higher than for cases 1 and 2. This conclusion is consistent with the 3D heat transfer numerical simulation and the high-speed images of the vapor detaching, for different flow mass rates and the input power.

The principal difference between the microchannel flow patterns observed here, and the well-accepted patterns observed in macro-tubes [19–21] is that no stratified flow appears to exist in the microchannels. This is the result of the combined effects of the gravitational body force, which is of relatively smaller significance and the surface tension, which plays a much more important role in the determination of the flow regime in microchannels. These two factors, coupled with the influence of the shape of the interface make the flow patterns and flow regimes different for these two different situations.

6. Conclusions

A new and promising experimental method is proposed, developed and utilized to investigate the liquid/vapor two-phase flow patterns in microchannels. This new method has several distinct advantages over previously used methodologies: (i) a single channel is fabricated and tested, eliminating any problems associated with the maldistribution of the flow; (ii) the stability of the flow is not influenced by the entrance and exit regions of the test section, thus the nature of the two-phase flow can be more clearly revealed; and (iii) the precise time dependent, geometric shape of the resulting two-phase flow is clearly revealed through high-speed

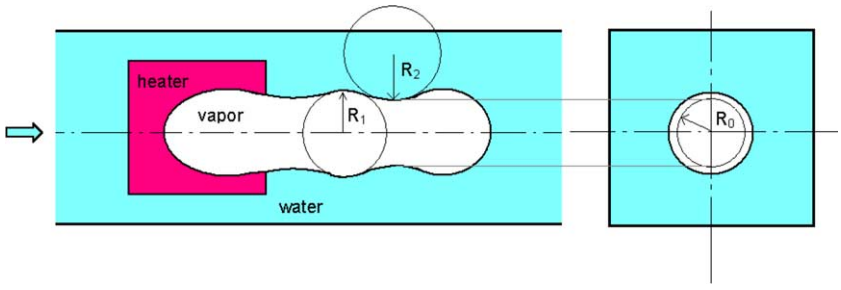

Fig. 14. Two-phase flow model in the microchannel based on the stability of the thin liquid film with evaporation or condensation.

synchronized photomicrography and temperature measurements.

A number of conclusions result: First, the characteristics of the heating surface can significantly affect the boiling incipience temperature. For a very smooth surface under forced flow situation, the temperature for vapor explosion is very close to or even higher than the theoretical value as predicted from the kinetics of nucleation. The nucleation temperature associated with the subcooled liquid flow rates should be studied further to explore whether and how the flow can influence the nucleation temperature. While adequate, the present experimental method to measure the temperature of the heater is not well suited for high flow rates, due to the nonuniformity of the temperature distribution under subcooled, forced convective flow.

The second and perhaps more important result is that the liquid/vapor two-phase pattern in microchannels can be identified from the present study using a local vapor generation method. It is clear that under low mass flow rates and low vapor generation rates, the flow will be bubbly flow; for moderate flow rates and moderate vapor generation rates, the flow will be wavy flow; and for large flow rates and vapor generation, the flow is annular flow. In all cases the various flow regimes were stable for long periods of time.

These results are in basic agreement with the liquid-vapor pattern maps in tubes proposed by Soliman [19,20] and Taitel–Dukler [21], except that for the absence of stratified flow, which was not be observed in the microchannels evaluated here. From the film stability analysis, it is clear that increasing the liquid flow rates can stabilize the vapor–liquid interface, which agrees with the present experimental observations.

While providing considerable clarification and insight to the behavior of these flows, considerable work remains, to further explore the transition regions and generate more detailed pattern maps for microchannel two-phase flow.

Acknowledgements

The authors would like to acknowledge the support of the Office of Naval Research Grant ONR N000140010454 and the National Science Foundation CTS-0312848. This work would not have been possible without earlier support by Prof. P. Cheng of the Hong Kong University of Science and Technology.

References

[1] X.F. Peng, B.X. Wang, Forced-convection and flow boiling heat transfer for liquid flowing through microchannels, Int. J. Heat Mass Transfer 36 (14) (1993) 3421–3427.
[2] X.F. Peng, B.X. Wang, Evaporation space and fictitious boiling for internal evaporation of liquid, Sci. Foundation China 2 (1994) 55–59.
[3] H.Y. Wu, P. Cheng, Visualization and measurements of periodic boiling in silicon microchannels, Int. J. Heat Mass Transfer 46 (14) (2003) 2603–2614.
[4] H.Y. Wu, P. Cheng, Boiling instability in parallel silicon microchannels at different heat flux, Int. J. Heat Mass Transfer 47 (17–18) (2004) 3631–3641.
[5] M. Lee, Y.Y Wong, M. Wong, Y. Zohar, Size and shape effects on two-phase flow patterns in microchannel forced convection boiling, J. Micromech. Microeng. 13 (2003) 155–164.
[6] L.A. Jiang, M. Wong, Y. Zohar, Forced convection boiling in a microchannel heat sink, J. Microelectromech. Syst. 10 (1) (2001) 80–87.
[7] G. Hetsroni, A. Mosyak, Z. Segal, E. Pogrebnyak, Two-phase flow patterns in parallel micro-channels, Int. J. Multiphase Flow 29 (3) (2003) 341–360.
[8] P.M.Y. Chung, M. Kawaji, A. Kawahara, Y. Shibata, Two-phase flow through square and circular microchannels—Effects of channel geometry, ASME J. Fluids Eng. 126 (4) (2004) 546–552.
[9] W.L. Qu, S.M. Yoon, I. Mudawar, Two-phase flow and heat transfer in rectangular micro-channels, J. Electron. Packaging 126 (3) (2004) 288–300.
[10] S.G. Kandlikar, Fundamental issues related to flow boiling in minichannels and microchannels, Exp. Thermal Fluid Sci. 26 (2–4) (2002) 389–407.
[11] G.E. Kendall, P. Griffith, A.E. Bergles, J.H. Lienhard, Small diameter effects on internal flow boiling, in: Proceedings of 2001 ASME International Mechanical Engineering Congress and Exposition, New York, 2001, pp. 1–17.
[12] P. Rao, R.L. Webb, Effects of Flow Mal-distribution in Parallel Micro-channels, in: Proceedings of 34th National Heat Transfer Conference, Pittsburgh, 2000, pp. 1–9.
[13] R. Cole, Boiling nucleationAdvances in Heat Transfer, 10, Academic Press Inc., 1974, pp. 86–166.
[14] J. Li, P. Cheng, Bubble cavitation in a microchannel, Int. J. Heat Mass Transfer 47 (2004) 2689–2698.
[15] A.W. Adamson, Physical Chemistry of Surface, John Wiley & Sons, New York, 1990.
[16] J.D. Parker, J.H. Boggs, E.F. Blick, Introduction to Fluid Mechanics and Heat Transfer, Addison-Wesley Publishing Company, Reading, MA, 1974.
[17] M.K. Dobson, J.C. Chato, Condensation in smooth horizontal tubes, ASME J. Heat Transfer 120 (1) (1998) 193–213.
[18] J. El Hajal, J.R. Thome, A. Cavallini, Condensation in horizontal tubes, Part 1: Two-phase flow pattern map, Int. J. Heat Mass Transfer 46 (2003) 3349–3363.
[19] H.M. Soliman, On the annular-to-wavy flow pattern transition during condensation inside horizontal tubes, The Can. J. Chem. Eng. 60 (1982) 475–481.
[20] H.M. Soliman, Correlation of the mist-to-annular transition during condensation, The Can. J. Chem. Eng. 61 (1983) 178–182.

[21] Y. Taitel, A.E. Dukler, A model for predicting flow regime transitions in horizontal and near horizontal gas–liquid flow, AIChE J. 22 (1) (1976) 47–55.
[22] E. Ruckenstein, R.K. Jain, Spontaneous rupture of thin liquid films, J. Chem. Soc. Faraday Trans. II 70 (1974) 132–147.
[23] J.P. Burelbach, S.G. Bankoff, S.H. Davis, Nonlinear stability of evaporating/condensing liquid film, J. Fluid Mech. 195 (1988) 463–494.
[24] J.M. Vandenbroeck, J.B. Keller, Deformation of a bubble or drop in a uniform-flow, J. Fluid Mech. 101 (1980) 673–686.